JOURNAL OF GEOPHYSICAL RESEARCH, VOL. 100, NO. D3, PAGES 5123–5132, MARCH 20, 1995

Validation of the NOAA/NESDIS satellite aerosol product over the North Atlantic in 1989

Aleksandr M. Ignatov[1] and Larry L. Stowe

National Oceanic and Atmospheric Administration/National Environmental Satellite Data and Information Service, Satellite Research Laboratory, Camp Springs, Maryland

Sergey M. Sakerin

Institute of Atmospheric Optics, Tomsk, Russia

Gennady K. Korotaev

Marine Hydrophysics Institute, Sevastopol, Ukraine

Abstract. A validation experiment and resulting potential improvements to the operational satellite aerosol optical thickness product at the National Oceanic and Atmospheric Administration/National Environmental Satellite Data and Information Service (NOAA/NESDIS) are presented. An earlier paper described a set of Sun photometer measurements collected from the Soviet R/V *Akademik Vernadsky* during its cruise in the Atlantic Ocean and Mediterranean Sea from September to December 1989. The accuracy of the Sun photometer aerosol optical thickness was proven acceptable for use as a ground truth standard for validation of the NOAA product. This paper describes the validation methodology and the results of its application to the NOAA 11 satellite product. A systematic underestimation in the operational values by about 35%, relative to the ship truth, is found. Causes for this discrepancy are examined, emphasizing the importance of careful satellite instrument calibration, and a revision of the oceanic reflectance model used in the retrieval algorithm. It is shown that the remaining systematic underestimate in satellite aerosol optical thickness can be attributed only to the aerosol model used in the retrieval. Additional checks of this conclusion using independent data sets are underway. If confirmed, a fundamental revision of the presently used aerosol model would be required. An example of a simple adjustment to the present aerosol model which successfully removes the bias is given, based on the assumption of an absorbing aerosol.

1. Introduction

The experimental production of aerosol optical thickness τ^A_{SAT} over oceans from NOAA polar orbiters began at National Oceanic and Atmospheric Administration/National Environmental Satellite Data and Information Service (NOAA/NESDIS) in July 1987 [*Rao et al.*, 1989] and became operational in January 1990 [*Stowe*, 1991]. This first-generation product, which makes use of measurements in only channel 1 (0.63 μm) of the advanced very high resolution radiometer (AVHRR/2), could possibly be improved. In particular, the measurements in channel 2 (0.85 μm) contain some additional information on aerosol [*Kaufman et al.*, 1990; *Durkee et al.*, 1991] which is not utilized by the present algorithm. However, before developing a second-generation product it is worthwhile knowing in detail the advantages and restrictions of the present single-channel algorithm. One means of achieving this knowledge is through validation experiments using Sun photometer (SP) measurements τ^A_{SP}. This had been done about 10 years earlier while developing the retrieval algorithm. Those studies indicated that a single-channel algorithm could retrieve aerosol optical thickness globally with little systematic error and with random errors between 0.03 and 0.05 [*Griggs*, 1983]. However, the quality of the Sun photometer was suspect, and the satellite analysis was done manually. Thus, to test the performance of the NOAA operational product, a new validation program has commenced, with an emphasis on collecting a reliable ground truth standard and thorough verification of each model assumption and parameter.

The τ^A_{SP} data collected during the cruise of the R/V *Akademik Vernadsky* from September to December 1989 (hereinafter AV-89) were evaluated by *Korotaev et al.* [1993] to be accurate to ± 0.02 in 3 SP channels at 0.48, 0.55, and 0.67 μm. In the present paper the methodology of validation and the result of its application to coincident NOAA 11 τ^A_{SAT} and AV-89 τ^A_{SP} data are presented. With this analysis, systematic errors are found to be much larger than in the earlier studies. The errors resulting from satellite sensor calibration errors and inadequacy of the oceanic reflectance model are corrected using data available in the scientific literature. The remaining multiplicative underestimation of about 2 times in τ^A_{SAT} can be attributed only to the aerosol model used in the retrieval. This result has to be further checked with independent data sets. If confirmed, this

[1]Also at Marine Hydrophysics Institute, Sevastopol, Ukraine.

Paper number 94JD03322.
0148-0227/95/94JD-03322$05.00

suggests that the aerosol model in the presently used operational algorithm must be revised. An example of a model change, reconciling the satellite and SP data, is given.

2. Operational Retrieval Algorithm

Aerosol retrievals are made from those average reflectances in channel 1 for 2 × 2 arrays of cloudless global area coverage (GAC) pixels, not contaminated by direct sun glint. The cloud-screening procedure is described by *McClain* [1989]. To avoid specular reflection (direct glint) from the ocean surface, only data from the antisolar side of the swath is used [*McClain*, 1989]. The NOAA 11 AVHRR actually receives some specular reflection on the antisolar side near nadir. A test was formulated to exclude this region. It is defined by the cone angle about the direction of specular reflection [*Stowe et al.*, 1991]. A value of 40° was found empirically to remove most of this unwanted source of surface reflection from the operational product.

In the model of *Rao et al.* [1989], aerosol over ocean is assumed to be nonabsorbing (refractive index $n = 1.5 - 0.0i$) and to obey a modified Junge size distribution

$$\begin{aligned} dN/dr &= 0 \qquad r < r_{\min} \qquad r > r_{\max} \\ dN/dr &= A \qquad r_{\min} \le r \le r_m \\ dN/dr &= A(r/r_m)^{-(v+1)} \qquad r_m \le r \le r_{\max} \end{aligned} \tag{1}$$

where $r_{\min} = 0.03$; $r_m = 0.1$; $r_{\max} = 10$ μm; $v = 3.5$ (corresponds to an equivalent Angstrom exponent $\alpha \approx 1.5$ [see *Liou*, 1980]). Elterman's vertical profile of aerosol concentration $A(h)$; midlatitude ozone profile with integrated ozone content of 0.316 atm cm; and Lambertian ocean with albedo $\rho^S = 0.015$ (1.5%) are assumed.

By specifying this model of the ocean-atmosphere system a unique relationship between τ^A_{SAT} and the upward reflectance can be established with a radiative transfer model. This fact underlies the present single-channel NOAA operational algorithm which uses a lookup table (LUT) to retrieve τ^A_{SAT} from satellite reflectances in AVHRR/channel 1, corrected to mean Sun-Earth distance. The LUT is precalculated for different illumination and observation geometries and aerosol loadings using the *Dave* [1973] radiative transfer code. In the operational algorithm, τ^A_{SAT} is retrieved at the wavelength of 0.63 μm and then scaled to 0.5 μm, consistent with the retrieval model.

Shortly after launch of the NOAA 11 in September 1988 it became clear that the operational calibration procedure for AVHRR/channel 1 was inconsistent with the physical algorithm of retrieval. This had been noted in earlier studies as well [*Griggs*, 1983; *Rao et al.*, 1989]. Without calibration correction, τ^A_{SAT} is underestimated (can even be negative) and tends to increase with latitude. An attempt was made to correct for both effects simultaneously by adding the following term to the observed reflectance (or "albedo" α_{op}):

$$\Delta\alpha = 2.135 - 0.0288\Theta_s \tag{2}$$

The percent albedo used in the NOAA practice is defined as $\alpha = 100\pi LWF_s^{-1}$, with L (W m^{-2} μm^{-1} sr^{-1}) being the measured upward radiance. The effective solar constant F_s and equivalent width W for AVHRR/channel 1 on NOAA 11 are $F_s = 184.1$ W m^{-2} (corresponds to mean Sun-Earth distance) and $W = 0.113$ μm [*Kidwell*, 1991]; Θ_s is the solar zenith angle in degrees. In case negative τ^A_{SAT} retrievals still occur they are replaced by zeros.

3. Construction of Matchup Dataset

When comparing any set of satellite and ground truth measurements one usually meets two problems: different spatial scales for the two measurements and lack of exact coincidence in space and time. These two difficulties, if improperly treated, could result in misinterpretation of the results. Here the principles used to form the merged data set are discussed.

To begin one needs to know the statistical structure of the field under analysis. Appropriate space-time correlation radii could be used to establish distance thresholds beyond which coincidence of satellite and ground data in both space and time are unacceptable. However, information on the statistical structure of aerosol fields over oceans is not available at present with sufficient accuracy. Instead, for the small number of matchup points under comparison, individual analyses are made to decide whether any particular point may be used for validation. The procedure of selecting validation points is as follows: from ~300 ground truth SP measurements taken during AV-89 in the North Atlantic and Mediterranean Sea [*Korotaev et al.*, 1993] the closest in time (within 3 hours of satellite overpass) are selected; then, 10 satellite retrievals nearest in space to the ship (within 300 km) are searched, each of them corresponding to an average of a cloud-free subsample of 2 × 2 GAC pixels [*McClain*, 1989].

Further analysis of this merged data set consists of studying both the spatial and temporal variability of aerosol optical thickness. On the average, five to six SP measurements were taken during each matchup day. These are used to estimate the temporal variability in τ^A_{SP}, because the distance traveled by the ship during 1 day is small. Two examples of such an analyses are given in Figures 1a and 1c for two selected days: October 5 and November 28, 1989, respectively. Figures 1b and 1d demonstrate the scattering of the 10 nearest satellite measurements around the ship track during these 2 days. Analysis of retrieved τ^A_{SAT} at these 10 points allows the spatial homogeneity of the aerosol field to be evaluated, as the measurements are almost instantaneous.

Figure 1a (October 5) shows that τ^A_{SP} almost doubled between the last two measurements. The ship apparently moved into a region of aerosol spatial inhomogeneity. The satellite data also show large variability in τ^A_{SAT} (standard deviation is 0.05, compared to a value of 0.02 typical of other matchups). Also, the satellite and ship measurements are separated by 200 km. For these reasons, this case is excluded from further analysis. Figures 1c and 1d give an example of a "good" matchup (November 28), where τ^A_{SP} was extremely stable, the satellite data are scattered around the ship track, and τ^A_{SAT} also satisfies the spatial uniformity criterion.

After application of this procedure, only 20 coincident ship/satellite matchups remain. These are listed in Table 1, together with the complete SP, satellite, and meteorological situation in each matchup point.

4. Analysis of the Matchup Dataset

In order to check correctness of the retrieval model, described in section 2, by comparison of τ_{SP}^{A} and τ_{SAT}^{A}, one can either calculate the upward albedo using τ_{SP}^{A} as input to the LUT and compare with the satellite albedo, or one can convert satellite albedo to a "radiatively equivalent" (i.e., radiative transfer model dependent) aerosol optical thickness τ_{SAT}^{A} using the LUT and compare it with τ_{SP}^{A}. In the present paper we follow the latter method. Also, we allow negative τ_{SAT}^{A} retrievals to analyze the physics of the phenomena more clearly.

In the present situation, when both sources of data under comparison are not exactly collocated or invariant in space, it is preferable to compare τ_{SP}^{A} and τ_{SAT}^{A} averaged over some space-time interval rather than choosing the closest in space and time. The noise in τ_{SP}^{A} and τ_{SAT}^{A} may result from both their natural variability and measurement errors. Also, the gridded NOAA operational product provides an objective analysis of τ_{SAT}^{A} fields over a (1° × 1°) × 1 week space-time box [*Stowe*, 1991]. For these reasons, a procedure based on comparing average values is more appropriate for validation of this product.

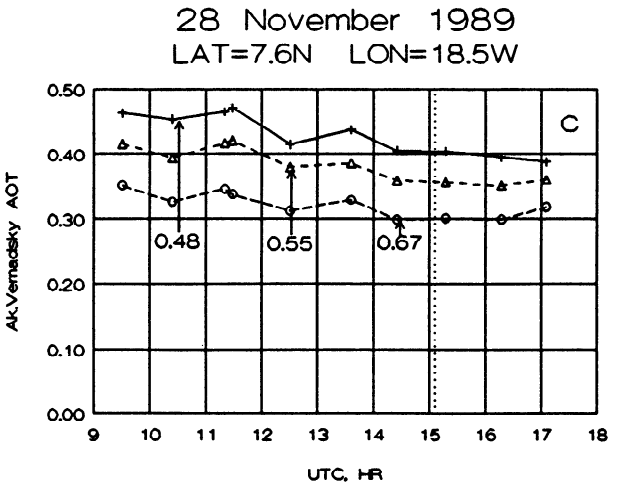

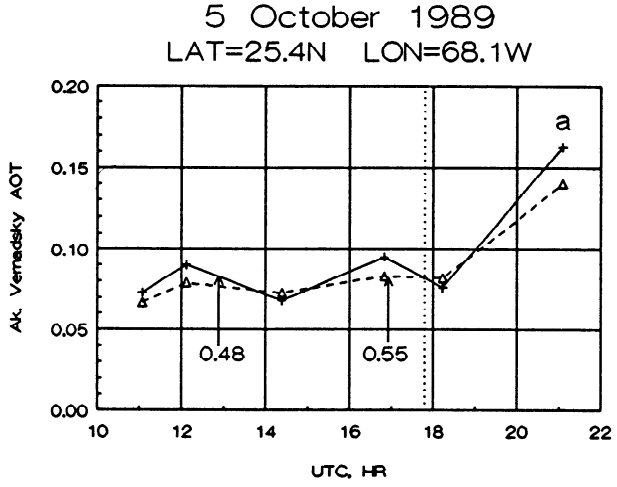

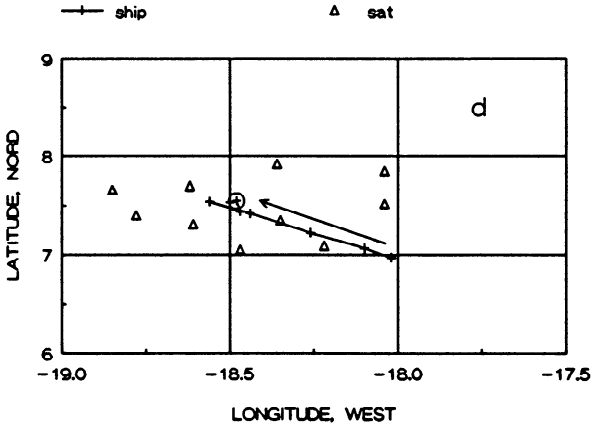

Figure 1. (continued)

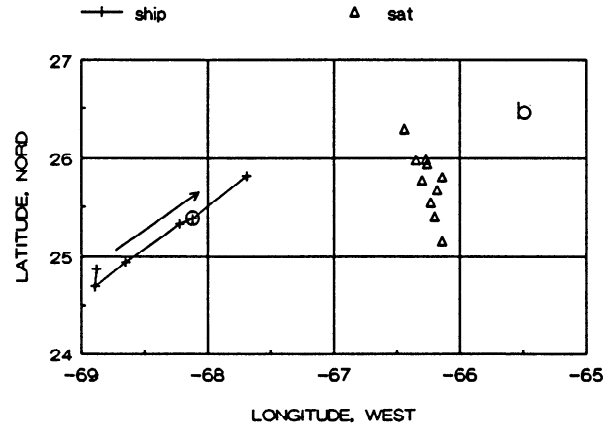

Figure 1. (a) Temporal variability of τ_{SP}^{A} at two wavelengths and (b) relative spatial position of the ship track and 10 subsatellite points during October 5, 1989. (c) Temporal variability of τ_{SP}^{A} at three wavelengths and (d) relative spatial position of the ship track and 10 subsatellite points during November 28, 1989. Vertical dotted line indicates time of satellite overpass. Circled point around ship track indicates the corresponding ship location. Arrow indicates the direction of the ship's motion.

For each of the 20 matchup points, all 10 satellite measurements are averaged, except for bright outliers. Averaging and removal of outliers, indicating residual cloud contamination, are carried out after conversion of the satellite albedo into τ_{SAT}^{A} using the operational algorithm [*Rao et al.*, 1989]. The mean τ_{SAT}^{A}, τ_0, and standard deviation σ_τ are calculated for each 10-point group, and the measurements with $\tau > \tau_0 + 2\sigma_\tau$ are excluded. This procedure is iteratively repeated until the points cease being excluded. The mean of the resulting compact cluster τ_0 with the uncertainty σ_τ are used further in the analysis.

Averaging of τ_{SP}^{A}, log-linearly interpolated to $\lambda = 0.50$ and 0.63 μm, is carried out over the measurements within ±2 hours of the satellite overpass. This is the time it would take a parcel of air to pass through a typical cluster of satellite measurements around the ship (about 30–50 km), if one assumes an average wind speed of 7 m s^{-1}.

Results of comparison of τ_{SAT}^{A} and τ_{SP}^{A} at $\lambda = 0.5$ μm are

Table 1. *Akademik Vernadsky* 89 Matchup Dataset Under Analysis

Case	Date	UTC, hour: Ship	UTC, hour: Satellite	Geographic Sun Photometer: Latitude	Geographic Sun Photometer: Longitude	τ_{SP}^{A}: 0.50 μm	τ_{SP}^{A}: 0.63 μm	Temperature, °C: Air	Temperature, °C: Water	Wind, m/s	Relative Humidity, percent	Clouds: Low	Clouds: High	DL: Mean	DL: Standard	Counts: Mean	Counts: Standard	Θ_s: Mean	Θ_s: Standard	Θ_v: Mean	Θ_v: Standard	ϕ: Mean	ϕ: Standard	Scatter: χ^-	Scatter: χ^+
A	Sept. 4	13.1	13.4	49.5N	3.5W	0.135	0.097	16.0	16.0	2.2	64	2	0	10	14	61.7	0.9	44.7	0.1	1.0	0	129	0.2	136	45
B	Sept. 10	11.9	14.1	59.8N	2.7E	0.049	0.036	11.2	12.5	2.6	66	0	0	84	21	72.0	0.4	59.9	0.2	57.3	0.8	129	0.1	137	101
C	Oct. 8	17.7	17.5	21.6N	57.0W	0.085	0.083	26.9	27.6	6.8	64	2	2	25	27	63.0	1.3	38.9	0.2	4.1	1.0	148	0.3	145	42
D	Oct. 9	16.9	17.3	20.0N	52.2W	0.046	0.046	27.3	27.8	9.1	71	3	1	23	31	66.8	1.2	39.6	0.2	16.8	2.3	150	0.3	154	55
E	Oct. 10	17.1	17.1	18.2N	47.1W	0.045	0.052	27.0	28.0	4.3	79	5	4	8	53	64.3	0.5	40.4	0.3	28.9	2.2	153	0.4	161	67
F	Oct. 12	16.7	16.7	15.1N	37.8W	0.272	0.270	27.7	27.5	9.3	80	5	4	59	74	87.5	2.3	41.9	0.6	45.7	2.7	158	0.5	165	86
G	Oct. 16	16.1	16.0	11.4N	26.0W	0.426	0.400	27.0	28.2	8.9	77	4	3	34	63	100.1	2.5	41.8	0.4	46.8	1.8	161	0.5	166	87
H	Oct. 17	16.0	15.8	11.7N	21.4W	0.485	0.455	27.6	28.4	7.0	76	2	2	146	176	102.6	2.2	43.1	0.6	50.3	1.8	160	1.7	164	92
I	Nov. 26	15.2	15.5	4.1N	18.0W	0.240	0.195	27.0	28.3	2.5	81	9	2	12	73	79.9	1.9	44.2	0.5	41.2	2.4	152	0.5	161	82
J	Nov. 28	15.3	15.1	7.6N	18.5W	0.390	0.316	28.4	29.1	4.3	79	1	1	9	43	73.0	0.8	42.1	0.3	6.1	2.1	145	0.3	143	47
K	Dec. 5	15.4	15.6	21.0N	18.3W	0.032	0.032	21.5	21.9	5.5	81	2	1	20	87	75.1	2.1	56.9	0.6	57.1	1.6	139	0.4	146	103
L	Dec. 6	15.3	15.4	22.0N	19.5W	0.111	0.113	20.5	22.7	5.4	69	5	1	43	86	70.4	2.4	55.7	0.6	43.7	2.5	136	0.3	145	90
M	Dec. 7	13.9	15.3	20.9N	17.4W	0.072	0.079	20.9	20.0	0.7	74	0	0	58	82	64.3	0.9	54.1	0.5	37.9	1.7	136	0.4	145	84
N	Dec. 8	14.6	15.1	22.5N	18.1W	0.044	0.053	22.3	22.2	3.7	73	6	0	12	48	60.4	1.5	53.9	0.4	23.4	2.4	134	0.2	140	71
O	Dec. 9	15.9	14.9	23.7N	16.8W	0.034	0.038	20.1	21.3	3.1	88	8	1	92	41	58.7	2.4	53.4	0.3	9.0	2.3	132	0.2	132	60
P	Dec. 10	15.8	14.8	27.5N	16.3W	0.040	0.052	20.3	21.4	7.7	88	7	3	57	56	57.0	1.1	56.0	0.3	4.3	2.9	130	0.4	127	59
Q	Dec. 15	13.5	13.9	35.3N	6.7W	0.039	0.043	18.5	18.9	4.9	83	3	2	105	40	57.4	1.6	63.3	0.1	2.2	2.1	125	0.4	118	65
R	Dec. 16	14.0	13.7	36.7N	0.7E	0.036	0.034	20.5		10.8	65			2	16	57.0	0.1	65.6	0.2	27.2	1.0	126	0.1	128	83
S	Dec. 17	13.6	13.5	37.3N	8.3E	0.124	0.134	21.0		4.2	65			2	25	67.5	3.1	67.9	0.1	48.9	1.1	128	0.2	132	100
T	Dec. 18	13.7	13.4	36.3N	15.5E	0.025	0.024	19.3		11.1	83			19	28	72.2	0.5	68.7	0.2	59.7	0.0	129	0.2	134	109

The columns indicate identification symbol for each matchup day and its date, UTC of satellite overpass and the nearest Sun photometer measurement, the latter's coordinates, τ_{SP}^{A} averaged over a few points closest to satellite overpass and interpolated to $\lambda = 0.5$ and 0.63 μm, air and sea surface temperature, 10 m wind speed, relative humidity, mean cloudiness (in tenths of sky cover) in the vicinity of the ship for low and high levels, remoteness of the centrum of the 10 satellite points cluster from the ship in kilometers (which is DL), count in AVHRR/channel 1, solar and view zenith angles Θ_s and Θ_v, relative azimuth ϕ ($\phi = 180°$ for backscatter), scattering angles χ^- and χ^+ (means and standard deviations are given for DL, counts, Θ_s, Θ_v, ϕ, χ^-, χ^+). See details in text.

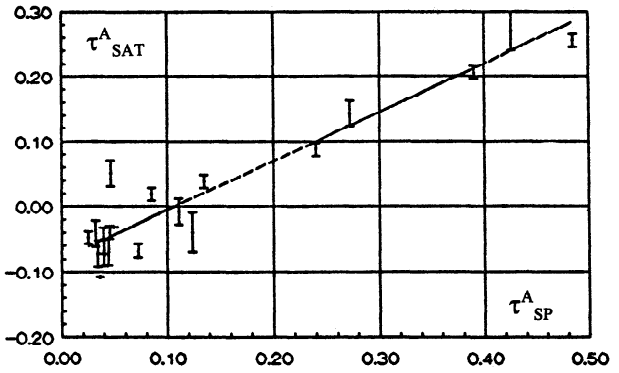

Figure 2. Operational τ^A_{SAT} versus τ^A_{SP} (λ = 0.5 μm). Regression analyses: $\tau^A_{SAT} < 0$ allowed: τ^A_{SAT} = (−0.081 ± 0.011) + (0.75 ± 0.06) τ^A_{SP}, σ = 0.036 and R^2 = 0.91; $\tau^A_{SAT} < 0$ replaced by 0: τ^A_{SAT} = (−0.035 ± 0.009) + (0.66 ± 0.05) τ^A_{SP}, σ = 0.029 and R^2 = 0.92.

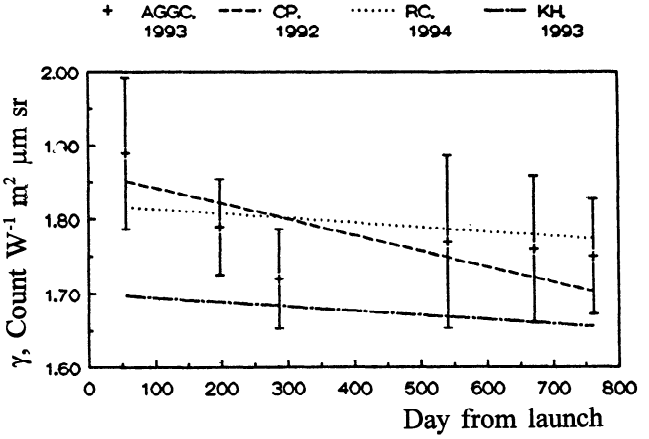

Figure 3. Comparisons of gain in AVHRR/channel 1 on board NOAA 11 from four literature sources: AGGC, 1993 [*Abel et al.*, 1993]; CP, 1992 [*Che and Price*, 1992]; RC, 1994 [*Rao and Chen*, 1994]; KH, 1993 [*Kaufman and Holben*, 1993]. The AV-89 experiment took place 350–450 days after the NOAA 11 launch.

presented in Figure 2. The τ^A_{SAT} values are obviously underestimated, relative to τ^A_{SP}, with 12 of 20 being negative. The regression analyses were performed for two cases: with allowed negative τ^A_{SAT} retrievals and with those replaced by zeros as is the operational practice. Both results are given in the Figure 2 caption. The discrepancy between τ^A_{SAT} and τ^A_{SP} clearly exceeds the uncertainty of 0.02 in τ^A_{SP} [*Korotaev et al.*, 1993] and must therefore result only from errors in the τ^A_{SAT} retrieval process. Three reasons may be responsible for these errors: incorrect satellite albedos, which are used as input to the retrieval algorithm; scaling of τ^A_{SAT} from λ = 0.63 μm to 0.5 μm; and inadequate physics in the retrieval model. In what follows, these sources of error are investigated in detail.

5. Recalibration of Satellite Radiances

AVHRR channels 1 and 2 are not calibrated in orbit. Their operational calibration consists of calculating spectral radiance L from the measured count C using formula $L = \gamma^{-1}(C - C_0)$, where the so-called gain γ (count W^{-1} m^2 μm sr) characterizes sensitivity of the sensor response; C_0 is the offset (dark count) registered by the satellite sensor when L = 0. In NOAA operational practice the preflight calibration constants γ = 2.128 and C_0 = 41.2 were used for AVHRR/channel 1 on board NOAA 11 before September 27, 1990, and γ = 2.029 and C_0 = 40.0 after that date [*Abel*, 1990; *Kaufman and Holben*, 1993]. The radiance L is further converted to NOAA albedo units α (percent) using the procedure described in section 2.

Recently, the results of postflight calibration studies of AVHRR/channel 1 on NOAA 11 were published [*Che and Price*, 1992; *Abel et al.*, 1993; *Kaufman and Holben*, 1993; *Rao and Chen*, 1994], and the opportunity presented itself to check the accuracy of the correction term of (2). Gains for AVHRR/channel 1 on NOAA 11 from these four sources are compared in Figure 3. For the time frames of the cruise (days 350–450 from launch of NOAA 11), degradation of the sensor is well within an uncertainty interval ≈±2% of the updated gain values (C. R. N. Rao, personal communication, 1994). We have accepted a constant of γ = 1.805 ± 0.035 according to *Rao and Chen* [1994]. The second calibration constant C_0 is in principle measured in-flight and is available on the NOAA 1b tapes [*Kidwell*, 1991]. However, as is the customary practice, a constant value of C_0 is used. According to *Kaufman and Holben* [1993], C_0 = 40 has been extremely stable on NOAA 11.

Thus the values of γ = 1.805 and C_0 = 40 are used for the recalibration of AVHRR/channel 1 during the total period of the AV-89 experiment. The result of using the recalibrated radiances in τ^A_{SAT} retrieval at λ = 0.5 μm is shown in Figure 4. The difference with Figure 2 is statistically insignificant and indicates that the empirical recalibration (2) is a reasonably good adjustment for the period of AV-89. A special sensitivity study showed that the uncertainty in gain value of $\delta\gamma \sim \pm 0.035$ (±2%) influences the retrieval of τ^A_{SAT} by $\delta\tau^A_{SAT} \sim \pm 0.01$.

6. Rescaling τ^A_{SAT} to λ = 0.63 μm

One of the possible sources of systematic error in the satellite data may be related to the scaling from a wavelength λ = 0.63 μm (AVHRR/channel 1) to a wavelength λ = 0.5 μm. This is done in a manner consistent with the radiative

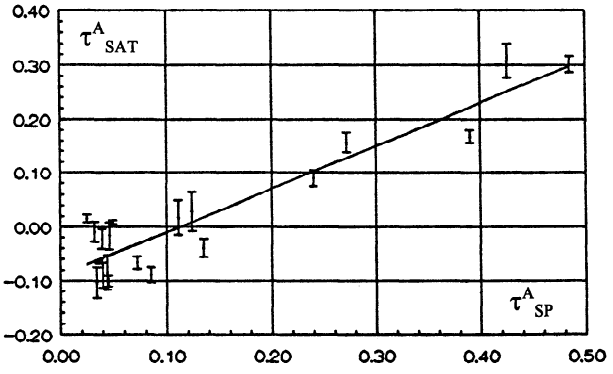

Figure 4. Same as Figure 2 but τ^A_{SAT} retrieved from recalibrated radiances (λ = 0.5 μm). Regression analysis: τ^A_{SAT} = (−0.089 ± 0.015) + (0.80 ± 0.07) τ^A_{SP}, σ = 0.047 and R^2 = 0.87.

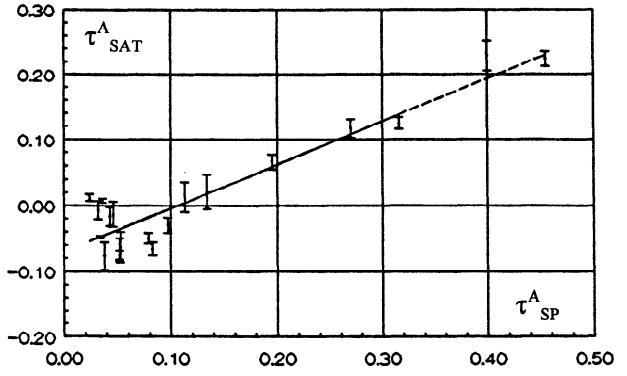

Figure 5. Same as Figure 4 but τ^A_{SAT} rescaled to $\lambda = 0.63$ μm. Regression analysis: $\tau^A_{SAT} = (-0.070 \pm 0.011) + (0.66 \pm 0.06)\ \tau^A_{SP}$, $\sigma = 0.034$ and $R^2 = 0.87$.

transfer model used for the retrieval at $\lambda = 0.63$ μm. To remove this possible source of error, which is atmospheric model dependent, all subsequent analyses are done at the wavelength of 0.63 μm. Eliminating this scaling error, the comparison results are shown in Figure 5. The systematic difference between the two data sets increased.

From the analyses in the latter two sections it follows that the reason for the discrepancy between the satellite and ground truth data is in the physics of the retrieval algorithm. In the next section we describe a simplified radiative transfer equation which is convenient for understanding the physical reasons for this error. We stress that it is used in the present paper only to guide the error analysis. Satellite retrievals in sections 8 and 9 are made using the rigorous radiative transfer model [*Dave*, 1973].

7. Simplified Radiative Transfer Equation

Comparison of τ^A_{SAT} with τ^A_{SP} for $\lambda = 0.63$ μm (Figure 5) shows the former to be underestimated. This manifests itself in both a pronounced negative bias $(\tau^A_{SAT} - \tau^A_{SP}) < 0$ and a slope of the regression line $d\tau^A_{SAT}/d\tau^A_{SP} < 1$. One has to draw the conclusion that the model of *Rao et al.* [1989] is inconsistent with this particular set of experimental data.

To identify the most plausible reasons for discrepancy, it is convenient to use the following decoupled form of the single-scattering approximation for the radiative transfer equation [*Tanré et al.*, 1979; *Viollier et al.*, 1980; *Gordon and Morel*, 1983]:

$$\rho = \rho^M + \rho^A + \rho^S T \tag{3}$$

where $\rho = \pi L W \mu_s^{-1} F_s^{-1}$ is an apparent reflectance at the top of the atmosphere ($\mu_s = \cos \Theta_s$). The relationship between ρ and the NOAA albedo α described in section 2 is $\rho = 0.01 \alpha \mu_s^{-1} d^2$, with d being the Sun-Earth distance in astronomical units. In (3), ρ^S is the diffuse oceanic reflection. Total (diffuse plus direct) atmospheric transmittance T may be approximated according to *Gordon and Clark* [1981] and *Gordon and Morel* [1983]

$$T = \exp\left(-[\tau^R/2 + (1 - \omega f)\tau^A][1/\mu_v + 1/\mu_s]\right) \tag{4}$$

where $\mu_v = \cos \Theta_v$ (Θ_v is view zenith angle); ω is the single-scattering albedo (maritime aerosol is usually assumed to be nonabsorbing, $\omega \approx 1$); f is the probability of forward scattering in a purely aerosol atmosphere. The ρ^R and ρ^A values describe Rayleigh and aerosol scattered contributions to ρ:

$$\rho^R = P^R \tau^R (4\mu_v \mu_s)^{-1}; \quad \rho^A = \omega P^A \tau^A (4\mu_v \mu_s)^{-1}$$

$$P^i = P^i(\chi^-) + [\rho_F(\mu_v) + \rho_F(\mu_s)] P^i(\chi^+) \tag{5}$$

where τ^i ($i = R, A$) are Rayleigh (R) and aerosol (A) optical thicknesses. For $\lambda = 0.63$ μm, $\tau^R \approx 0.06$ [*Liou*, 1980]. The generalized phase functions P^i include Fresnel reflection from a flat surface, ρ_F. The angle χ^- is measured between the vector from the Sun through the viewed pixel on the surface and the vector through the pixel to the satellite. The second term on the right-hand side of (5) accounts for the diffuse glint: that part of the measured radiation which is specularly reflected from the sea surface and scattered in the atmosphere before or after Fresnel reflection [*Gordon and Morel*, 1983]. The angle χ^+ is measured between the vector of directly reflected sunlight (glint) and the vector through the pixel to the satellite. Because of the reciprocity principle the scattering angle for the "scattering-before-reflection" case is the same as for "scattering-after-reflection." Gaseous absorption is neglected in the present analytical formulation for the sake of simplicity.

The described model can be summarized, for convenience of further analysis, in the resultant equation for τ^A_{SAT} retrieval:

$$\tau^A_{SAT} = [\rho - \rho^R - \rho^S T](4\mu_v \mu_s)(\omega P^A)^{-1} \tag{6}$$

Equation (6) allows one to analyze qualitatively the possible causes of errors in τ^A_{SAT}. The Rayleigh component, ρ^R, is well known. The atmospheric transmittance is also well constrained since from (4) it follows that $T \geq 0.8$ for typical illumination-observation geometries ($\mu_v \approx \mu_s \approx 0.7$), moderate $\tau^A_{SAT} \approx 0.2$, and $[1 - \omega f] \approx 0.13$ [*Viollier et al.*, 1980]. Additionally, analysis of the next section shows that $\rho^S \approx 0.002$ and thus the uncertainty in T (0.8–1.0) has a negligible effect on the error in the τ^A_{SAT} retrieval. Therefore errors in τ^A_{SAT} may result from incorrect ρ^S, ω, and/or P^A. Note that the oceanic diffuse reflectance ρ^S participates in (6) as an additive term and (ωP^A) as a multiplicative one. This suggests that the negative bias, $(\tau^A_{SAT} - \tau^A_{SP}) < 0$, in the operational satellite retrieval comes from overestimating the oceanic reflectance and the depressed slope $d\tau^A_{SAT}/d\tau^A_{SP} < 1$ from an incorrect atmospheric model (ω and/or P^A). We examine these possibilities in the next two sections using results from the simplified (6) for guidance. The satellite retrievals used in the matchup analysis are computed from the rigorous radiative transfer code [*Dave*, 1973] after making modifications suggested by this guidance.

8. Oceanic Reflectance

The oceanic model used by *Rao et al.* [1989] seems inadequate in two respects: it overestimates the diffuse component ρ^S for typical oceanic conditions and disregards the effect of Fresnel reflection of diffuse radiation from the surface, which is diffuse glint.

8.1. Diffuse Lambertian Reflectance

From (6) one can estimate the sensitivity of the retrieved τ^A_{SAT} to the parameter ρ^S:

$$\partial \tau^A_{\mathrm{SAT}}/\partial \rho^S = 4\mu_v \mu_s T(\omega P^A)^{-1} \quad (7)$$

For typical geometrical ($\mu_v \approx \mu_s \approx 0.7$) and atmospheric conditions ($\omega \approx 1$; $T \approx 0.9$; $P^A \approx 0.2$; for the latter see, e.g., *Viollier et al.* [1980]) one obtains $\partial \tau^A_{\mathrm{SAT}}/\partial \rho^S \approx 10$, which means that for the error in diffuse reflectance of $\delta\rho^S \sim 0.01$ one obtains an 0.1 error in τ^A_{SAT}. Thus the negative bias ($\tau^A_{\mathrm{SAT}} - \tau^A_{SP}$) ~ -0.07 could be caused by overestimating the ocean albedo by about 0.01. In what follows, a value for ρ^S is independently estimated from a survey of scientific literature.

The diffuse component of surface reflectance, ρ^S, is formed from two components: underlight ρ^S_U and foam reflectance ρ^S_f as $\rho^S = \rho^S_U + \rho^S_f$.

Underlight. According to *Gordon and Clark* [1981], *Gordon and Morel* [1983], and *Gordon et al.* [1988], ρ^S_U may be calculated from the subsurface irradiance ratio R (a measurable quantity in oceanology) by

$$\rho^S_U = (\pi/Q)\{[(1 - \rho_F)(1 - \langle \rho_F \rangle)]/n_w^2\}R \quad (8)$$

where Q is the angular distribution factor; $Q = \pi$ in the case of a perfectly diffuse reflector and $Q \approx 4.55 \pm 0.15$ for the real ocean [*Austin*, 1979]; $\rho_F \approx 0.04 \pm 0.02$ for a typical retrieval illumination-observation geometry; $\langle \rho_F \rangle \approx 0.05 \pm 0.02$ is the angular mean Fresnel albedo of the ocean; $n_w = 1.34$ is the refractive index of water for the AVHRR/channel 1 spectral range [*Hale and Querry*, 1973]. Substituting these values into (8) gives $\rho^S_U = (0.35 \pm 0.03)\,R$.

Spectral peculiarities of the subsurface irradiance ratios are described by *Morel and Prieur* [1977] and *Morel* [1980]. They summarized information on R obtained from 81 experiments in various types of waters representative of the global ocean. For the spectral range of the AVHRR/channel 1, typical values of R fall between 0.2 and 3.0%. According to (8) this is equivalent to $\rho^S_U = (0.55 \pm 0.50)\%$. According to the above estimates the uncertainty $\delta\rho^S_U \approx \pm 0.50\%$ can result in τ^A_{SAT} retrieval error up to $\delta\tau^A_{\mathrm{SAT}} \sim \pm 0.05$. This error is unacceptably large and requires narrowing the uncertainty in ρ^S_U values.

This can be done using the so-called concept of clear water radiances [*Morel and Prieur*, 1977; *Gordon and Clark*, 1981; *Gordon and Morel*, 1983]. According to this concept, seawater can be classified into two basic types: case 1 being those for which phytoplankton and their derivative products play a dominant role in determining the optical properties of the ocean and case 2, for which inorganic and/or organic sediments make an important or dominant contribution to the optical properties.

Open ocean waters belong, as a rule, to case 1 [*Gordon and Morel*, 1983]. They are also present in coastal areas off the continental shelf in the absence of terrigenious influence. Typical spectra for case 1 waters reveal variability in the blue-green (0.4–0.55 μm) part of the spectrum from oligotrophic (low pigment concentration, blue color) to eutrophic (high pigment concentration, green color) waters [*Morel and Prieur*, 1977]. Slight variability takes place also near 0.68 μm in the vicinity of a chlorophyll absorption line. However, over most of the AVHRR/channel 1 spectral range (0.58–0.68 μm) variability of R for case 1 waters is negligible, its typical values falling between 0.2 and 0.5%. Using (8), one obtains $\rho^S_U = 0.14 \pm 0.06\%$.

If these values of ρ^S_U are used over case 2 waters (mostly coastal regions: shelf, estuaries, or shallow banks), the underestimated oceanic diffuse reflectance would result in overestimating the retrieved τ^A_{SAT}. The single-channel algorithm cannot separate oceanic from atmospheric contributions to satellite radiance. To do this, additional a priori information on ocean color is necessary as input to the aerosol retrieval algorithm. However, this topic falls beyond the scope of the present validation study.

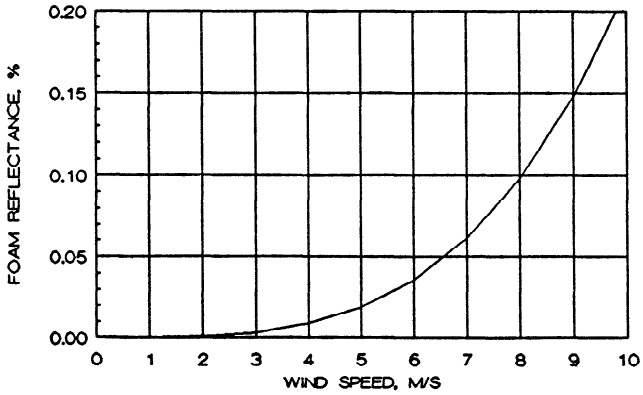

Figure 6. Reflectance of the foam (percent) as a function of wind speed U (meters per second) for the spectral interval of AVHRR/channel 1. Calculated using [*Koepke*, 1984] considerations.

Foam. Foam on the surface increases ocean reflectivity [*Koepke*, 1984]. Usually, foam is assumed to be an isotropic reflector. Total reflectance of the ocean foam ρ^S_f is a product of the relative area covered by whitecaps W and effective foam reflectivity ρ^{ef}_f, as $\rho^S_f = W\rho^{ef}_f$. An expression for W as a function of 10 m elevation wind U (m s^{-1}) is given by *Monahan and O'Muircheartaigh* [1980]: $W = 2.95 \times 10^{-6} U^{3.52}$. The spectral reflectance of a dense fresh foam of clear water $\rho^{\mathrm{fresh}}_f(\lambda)$ is ~55% for wavelengths up to $\lambda \sim 0.8$ μm as measured by *Whitlock et al.* [1982] in laboratory conditions. *Koepke* [1984] investigated experimentally the relation between ρ^{ef}_f and ρ^{fresh}_f. He drew attention to the fact that the area of an individual whitecap increases with its age while its reflectance decreases. Since whitecaps of different ages are taken into consideration in computing the W value, its combination with ρ^{fresh}_f results in an overestimate of the ρ^{ef}_f values. *Koepke* [1984] found out experimentally that $\rho^{ef}_f = \beta\rho^{\mathrm{fresh}}_f$ with factor β being ~0.4 ± 0.2 independent of wind speed and spectral interval. Combination of the latter value of β with the ρ^{fresh}_f values of *Whitlock et al.* [1982] gives $\rho^{ef}_f \approx 22 \pm 11\%$ for the AVHRR/channel 1 spectral range. The results of its use, together with W from *Monahan and O'Muircheartaigh* [1980], for the ρ^S_f calculation, are shown in Figure 6 versus wind speed U. For moderate wind speeds of 5–8 m s^{-1}, typical over most oceans, the value of ρ^S_f is (0.06 ± 0.04)%.

Thus this analysis of diffuse reflectance suggests that a value of $\rho^S = (0.2 \pm 0.1)\%$ is appropriate input to a radiative transfer model for aerosol retrieval over open ocean from AVHRR/channel 1 measurements. The remaining uncertainty $\delta\rho^S \sim \pm 0.1\%$ can result in τ^A_{SAT} errors of ~±0.01 according to the above sensitivity analysis.

The effect of using this diffuse reflectance factor in the retrieval model is illustrated in Figure 7. It does not significantly influence the slope $d\tau^A_{\mathrm{SAT}}/d\tau^A_{\mathrm{SP}} < 1$ as expected from

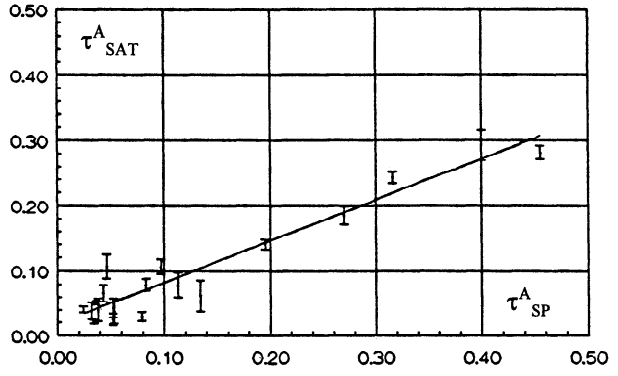

Figure 7. Same as Figure 5 but τ^A_{SAT} retrieved using model with $\rho^S = 0.2\%$ ($\lambda = 0.63$ μm). Regression analysis: $\tau^A_{SAT} = (0.017 \pm 0.008) + (0.63 \pm 0.04)\ \tau^A_{SP}$, $\sigma = 0.025$ and $R^2 = 0.92$.

the analysis in section 7. However, instead of negative bias ($\tau^A_{SAT} - \tau^A_{SP}$) ≈ -0.07 one obtains a positive one of the order of $\sim +0.02$. In the next subsection the effect of including diffuse glint in the retrieval algorithm is analyzed.

8.2. Diffuse Glint

The original Dave code assumes the underlying surface to be Lambertian and does not allow characterization of its bidirectional properties. To include the effects of specular reflection of diffuse skylight from a flat sea surface, the single-scattering approximation, described in section 7, has been used. Namely, "new" reflectances ρ_{new} were calculated from the "old" LUT values ρ_{old} using the formula

$$\rho_{new} = \rho_{old} + \Delta\rho^R + \Delta\rho^A,$$

$$\Delta\rho^i = \omega^i \tau^i [\rho_F(\mu_v) + \rho_F(\mu_s)] P^i(\chi^+) T^{oz}(\mu_v, \mu_s) \cdot (4\mu_v\mu_s)^{-1} \quad (9)$$

where $i = R$ or A; the aerosol phase function $P^A(\chi^+)$ was calculated using the Dave code; the Rayleigh phase function is $P^R(\chi^+) = \frac{3}{4}(1 + \cos^2\chi^+)$; $\omega^R \equiv 1$; $\omega^A = 1$ for the case of a nonabsorbing atmosphere; T^{oz} is the round-trip ozone transmission; Fresnel's reflection coefficient was calculated as the average of the two polarization components $\rho_F(\mu) = 0.5[\rho_F^{\perp}(\mu) + \rho_F^{\parallel}(\mu)]$ for natural unpolarized light. The $\rho_F^{\perp}$ and $\rho_F^{\parallel}$ values were calculated from Fresnel's classical formula, assuming the refractive index of the seawater to be $n_w = 1.34 - 0i$ [*Hale and Querry*, 1973].

The effect of including this treatment of the diffuse glint on τ^A_{SAT} retrieval is presented in Figure 8. The positive bias in τ^A_{SAT} is removed. The slope of the regression line remains the same and may be explained only by errors in the aerosol model, i.e., an incorrect (ωP^A) product being used in (6).

9. Aerosol Model

Incorrect P^A or ω results from an incorrect aerosol model. The presently used algorithm assumes particles to be spherical and to obey a modified Junge size distribution (1) with fixed parameters of r_{min}, r_m, r_{max}, v, and refractive index. Failure of any of these assumptions may result in τ^A_{SAT} errors (changes in the vertical aerosol distribution and/or in ozone content introduce at most 5% errors in τ^A_{SAT} [*Griggs*, 1983] and cannot be responsible for the matchup error). Adjusting the microphysical parameters to reconcile τ^A_{SAT} and τ^A_{SP} is very difficult because of so many degrees of freedom. The product (ωP^A) can be estimated from the matchup data, since both ρ and τ^A_{SP} are known as are the other terms in (6). It may be further interpreted in terms of a microphysical model using Mie theory or a more sophisticated approach [e.g., *Pollack and Cuzzi*, 1980]. This procedure is continuing to be investigated, and the results will be published elsewhere. For this paper one of several possible versions of the operational procedure is tested, which requires minor adjustments to its atmospheric model. Sphericity of the particles is assumed, and the Junge size parameter v and imaginary part of aerosol index of refraction Im(n) are adjusted to get agreement between τ^A_{SAT} and τ^A_{SP}.

First, the size parameter v is changed to correspond better with the experimental SP data. The narrow spectral range covered by SP channels with accurate measurements (0.48–0.67) and the smallness of τ^A_{SP} in many cases under analysis does not allow the hypothesis of a Junge-type size distribution to be checked in each individual matchup. The spectral dependence of τ^A_{SP} in the case of Junge's size distribution is known to obey Angstrom's law $\tau^A_{SP}(\lambda) \sim \lambda^{-\alpha}$, with $\alpha \approx (v - 2)$ being Angstrom's exponent. An effective α may be estimated from τ^A_{SP}, e.g., from regressions of $\tau^A_{SP}(\lambda_i)$ versus $\tau^A_{SP}(\lambda_j)$ which are given by *Korotaev et al.* [1993]. This analysis shows that the mean Angstrom exponent is $\alpha \approx 0.6$ over an ensemble of approximately 300 SP measurements taken during AV-89 in the spectral region 0.48–0.67 μm (in the vicinity of 0.63 μm). Note that the implication of a more neutral spectral dependence of aerosol optical thickness than that being assumed in the model compares well with data of other authors over the ocean [e.g., *Shifrin*, 1992]. Thus a more appropriate mean effective value for the Junge exponent is closer to $v \approx 2.5$ rather than 3.5 as used in the operational model (presently, we have chosen from three Junge parameters (1.5, 2.5, and 3.5) for which precalculated data were available). The effect of replacing this parameter is shown in Figure 9. Interestingly, this results in a further decrease in the slope, implying an inconsistency between the postulate of spherical particles, and/or the Junge size distribution, with the SP measurements.

The most obvious way to provide agreement between satellite and SP data is to increase the imaginary part of the

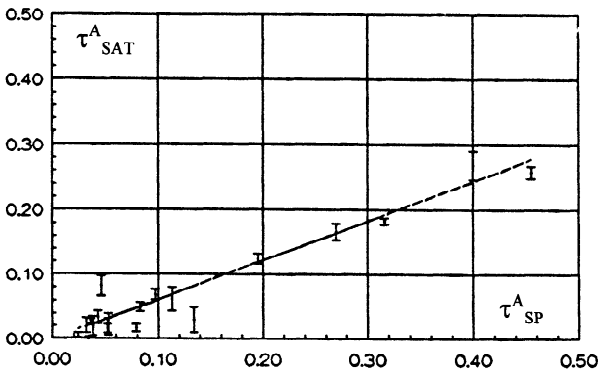

Figure 8. Same as Figure 7 but τ^A_{SAT} retrieved using model with diffuse glint ($\lambda = 0.63$ μm). Regression analysis: $\tau^A_{SAT} = (-0.004 \pm 0.007) + (0.61 \pm 0.04)\ \tau^A_{SP}$, $\sigma = 0.022$ and $R^2 = 0.93$.

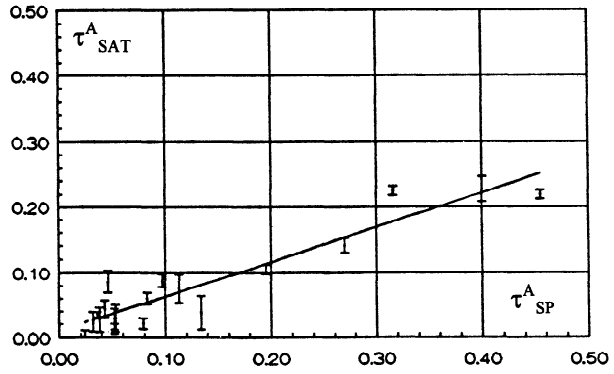

Figure 9. Same as Figure 8 but τ^A_{SAT} retrieved using model with $v = 2.5$ ($\lambda = 0.63$ μm). Regression analysis: $\tau^A_{SAT} = (0.007 \pm 0.008) + (0.53 \pm 0.04)\ \tau^A_{SP}$, $\sigma = 0.025$ and $R^2 = 0.89$.

aerosol's index of refraction. The reason for this is that a Sun photometer measures total aerosol extinction (absorption plus scattering), whereas the satellite radiometer senses only what is scattered. Thus increasing aerosol absorption in the retrieval model (i.e., $\omega < 1$ in equation (6)) should increase τ^A_{SAT} retrievals. Using $n = 1.5 - 0.01i$, one indeed gets almost perfect agreement between satellite and SP data as shown in Figure 10. Calculations give a value of the albedo of single scattering $\omega \approx 0.9$ for $v \approx 2.5$. For that value of ω, (6) predicts only ≈10% increase in τ^A_{SAT}. Further analysis has shown that P^A in the analyzed range of scattering angles decreases by up to ≈30% when this absorption is introduced. Both effects, decrease in P^A and ω, work together toward a pronounced increase of τ^A_{SAT}, bringing it into agreement with τ^A_{SP}. Since this result is in apparent contradiction with the present understanding of oceanic aerosols as an almost purely scattering substance (see, e.g., *D'Almeida et al.* [1991]), it may be that Saharan dust or smoke from agricultural burning was present, as most of the matchup points with large turbidity were taken in the tropical Atlantic Ocean. Both dust and smoke can have single-scattering albedo values near or even below 0.9 [*Takamura et al.*, 1984; *Nakajima et al.*, 1986; *D'Almeida et al.*, 1991]. The results of the present section show one of several possible ways to reconcile satellite and Sun photometer measurements. Investigations of alternative hypotheses are now underway.

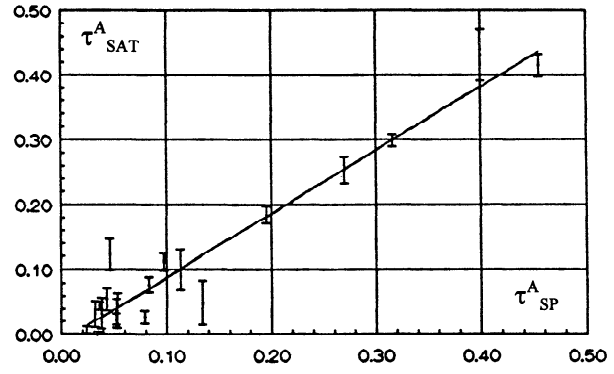

Figure 10. Same as Figure 9 but τ^A_{SAT} retrieved using model with Im(n) = 0.01 ($\omega \approx 0.9$, $\lambda = 0.63$ μm). Regression analysis: $\tau^A_{SAT} = (-0.008 \pm 0.011) + (0.98 \pm 0.06)\ \tau^A_{SP}$, $\sigma = 0.033$ and $R^2 = 0.94$.

10. Conclusion

Analysis of the matchup data set for *Akademik Vernadsky*-89 reveals an underestimation in the operational NOAA/NESDIS aerosol optical thickness retrieval algorithm of about 35%. After careful recalibration of the satellite data and correction of the oceanic reflectance model the remaining multiplicative underestimation in τ^A_{SAT} can be attributed only to the aerosol model used in the retrieval algorithm. The high correlation between the two data sets suggests that simple adjustments to the current aerosol model will, to a first approximation, bring the data analyzed in this paper into agreement. An example of two such adjustments is one increasing the proportion of large particles, which is consistent with the wavelength dependence of aerosol optical thickness measurements by the Sun photometer, and the other increasing particle absorption.

Combining traditional Sun photometer data with satellite measurements of upward reflectance has been shown to provide new insight into atmospheric aerosol properties not accessible from ground-based or satellite data alone. Further similar investigations, but with additional in situ measurements to specify the aerosol microphysical parameters, being planned within the International Global Aerosol and Global Atmospheric Chemistry Programs [*International Global Aerosol Program*, 1994; *Charlson*, 1992] are needed to confirm these findings and to establish the most appropriate aerosol model for satellite remote sensing. With this model the full potential of multispectral remote sensing methods as a means for detecting particle size changes and to account for these changes in optical thickness retrievals can be realized.

Acknowledgments. The authors thank R. Singh from the S. M. Systems and Research Corp. for performing the computations with the radiative transfer code. Sun photometer measurements were processed and prepared for validation by I. Dergileva from MHI. Advice of D. Tanré (University of Lille, France) concerning the diffuse glint problem is appreciated. Discussions with N. Rao (SRL) and S. Parshikov and E. Shibanov (MHI) while preparing the manuscript, and comments of anonimous reviewers and R. Mitchell (CSIRO, Australia) during its revision were very helpful. This investigation was carried out when A. I. held a National Research Council Associateship at NOAA/SRL, on leave from MHI.

References

Abel, P., Prelaunch calibration of the NOAA-11 AVHRR visible and near IR channels, *Remote Sens. Environ.*, *31*, 227–229, 1990.

Abel, P., B. Guenther, R. N. Galimore, and J. W. Cooper, Calibration results for NOAA-11 AVHRR channels 1 and 2 from congruent path aircraft observations, *J. Atmos. Oceanic Technol.*, *10*, 493–508, 1993.

Austin, R. W., Coastal zone color scanner radiometry, in Ocean Optics VI, *Proc. Soc. Photo Opt. Instrum. Eng.*, *208*, 170–177, 1979.

Charlson, R. J., *Multiphase Atmospheric Chemistry (MAC)*, 15 pp., International Global Atmospheric Chemistry Core Project Office Massachusetts Institute of Technology, Cambridge, 1992.

Che, N., and J. C. Price, Survey of radiometric calibration results and methods for visible and near infrared channels of NOAA-7, -9, and -11 AVHRRs, *Remote Sens. Environ.*, *41*, 19–27, 1992.

D'Almeida, G. A., P. Koepke, and E. Shettle, *Atmospheric Aero-*

sols: Global Climatology and Radiative Characteristics, 561 pp., A. Deepak, Hampton, Va., 1991.

Dave, J. V., Development of the programs for computing characteristics of ultraviolet radiation: Scalar case, *Rep. NAS5-21680*, NASA Goddard Space Flight Cent., Greenbelt, Md., 1973.

Durkee, P. A., F. Pfeil, E. Frost, and R. Shema, Global analysis of aerosol particle characteristics, *Atmos. Environ., Part A, 25*, 2457–2471, 1991.

Gordon, H. R., and D. K. Clark, Clear water radiances for atmospheric correction of coastal zone color scanner imagery, *Appl. Opt., 20*, 4175–4180, 1981.

Gordon, H. R., and A. Y. Morel, *Remote Assessment of Ocean Color for Interpretation of Satellite Visible Imagery: A review*, 114 pp., Springer-Verlag, New York, 1983.

Gordon, H. R., O. B. Brown, R. H. Evans, J. W. Brown, R. C. Smith, K. S. Baker, and D. K. Clark, A semianalytic radiance model of ocean color, *J. Geophys. Res., 93*, 10,909–10,924, 1988.

Griggs, M., Satellite measurements of tropospheric aerosols, *Adv. Space Res., 2*(5), 109–118, 1983.

Hale, G. M., and M. R. Querry, Optical constants of water in the 200-nm to 200-μm wavelength region, *Appl. Opt., 12*, 555–563, 1973.

International Global Aerosol Program, *A Plan for an International Global Aerosol Program*, edited by P. Hobbs, 54 pp., University of Washington, Seattle, 1994.

Kaufman, Y. J., and B. N. Holben, Calibration of the AVHRR visible and near-IR bands by atmospheric scattering, ocean glint and desert reflection, *Int. J. Remote Sens., 14*, 21–52, 1993.

Kaufman, Y. J., R. S. Fraser, and R. A. Ferrare, Satellite measurements of large-scale air pollution: Methods, *J. Geophys. Res., 95*, 9895–9909, 1990.

Kidwell, K., *NOAA Polar Orbiter Data Users Guide*, 154 pp., National Oceanic and Atmospheric Administration, Washington, D. C., 1991.

Koepke, P., Effective reflectance of oceanic whitecaps, *Appl. Opt., 23*, 1816–1824, 1984.

Korotaev, G., S. Sakerin, A. Ignatov, L. Stowe, and P. McClain, Sun-photometer observations of aerosol optical thickness over the North Atlantic from soviet research vessel for validation of satellite measurements, *J. Atmos. Oceanic Technol., 10*, 725–735, 1993.

Liou, K.-N., *An Introduction to Atmospheric Radiation*, 392 pp., Academic, San Diego, Calif., 1980.

McClain, P., Global sea surface temperatures and cloud clearing for aerosol optical depth estimates, *Int. J. Remote Sens., 10*, 763–769, 1989.

Monahan, E. C., and I. O'Muircheartaigh, Optimal power law description of oceanic whitecap coverage dependence on wind speed, *J. Phys. Oceanogr., 10*, 2094–2099, 1980.

Morel, A., In-water and remote measurements of ocean color, *Boundary Layer Meteorol., 18*, 177–201, 1980.

Morel, A., and L. Prieur, Analysis of variations in ocean color, *Limnol. Oceanogr., 22*, 709–722, 1977.

Nakajima, T., T. Takamura, M. Yamano, M. Shiobara, T. Yamauchi, R. Goto, and K. Murai, Consistency of aerosol size distribution inferred from measurements of solar radiation and aerosols, *J. Meteorol. Soc. Jpn., 64*(5), 765–776, 1986.

Pollack, J. B., and J. N. Cuzzi, Scattering by non-spherical particles of size comparable to a wavelength: A new semi-empirical theory and its application to tropospheric aerosols, *J. Atmos. Sci., 37*, 868–881, 1980.

Rao, C. R. N., and J. Chen, Post-launch calibration of the visible and near IR channels of AVHRR on NOAA-7, -9, and -11 spacecraft, *Tech. Rep. 78*, 22 pp., Natl. Oceanic and Atmos. Admin., Washington, D. C., 1994.

Rao, C. R. N., L. Stowe, and P. McClain, Remote sensing of aerosols over oceans using AVHRR data: Theory, practice and applications, *Int. J. Remote Sens., 10*, 743–749, 1989.

Shifrin, K. S., Optical properties of the atmosphere over ocean, in Optics of the Air-Sea Interface, *Proc. SPIE Int. Soc. Opt. Eng., 1749*, 151–164, 1992.

Stowe, L. L., Cloud and aerosol products at NOAA/NESDIS, *Paleogeogr. Paleoclimatol. Paleoecol., 90*, 25–32, 1991.

Stowe, L. L., E. P. McClain, R. Carey, P. Pellegrino, G. G. Gutman, P. Davis, C. Long, and S. Hart, Global distribution of cloud cover derived from NOAA/AVHRR operational satellite data, *Adv. Space Res., 11*(3), 51–54, 1991.

Takamura, T., M. Tanaka, and T. Nakajima, Effects of atmospheric humidity on the refractive index and the size distribution of aerosols as estimated from light scattering measurements, *J. Meteorol. Soc. Jpn., 62*(3), 573–582, 1984.

Tanré, D., M. Herman, P. Y. Deshamps, and A. de Leffe, Atmospheric modeling for space measurements of ground reflectances, including bidirectional properties, *Appl. Opt., 18*, 3587–3594, 1979.

Viollier, M., D. Tanré, and P. Y. Deshamps, An algorithm for remote sensing of water color from space, *Boundary Layer Meteorol., 18*, 247–267, 1980.

Whitlock, C. H., D. S. Bartlett, and E. A. Gurganus, Sea foam reflectance and influence of optimum wavelength for remote sensing of oceanic aerosols, *Geophys. Res. Lett., 9*, 719–722, 1982.

A. Ignatov and L. Stowe, NOAA/NESDIS/E/RA11, NSC Room 711, 5200 Auth Rd., Camp Springs, MD 20746.

G. Korotaev, Marine Hydrophysics Institute, Sevastopol 335005, Crimea, Ukraine.

S. Sakerin, Institute of Atmospheric Optics, Tomsk 634055, Siberia, Russia.

(Received July 12, 1994; revised October 25, 1994; accepted December 8, 1994.)